Effect of fused silica subsurface defect site density on light intensification*

Li Li(李 莉)[a)†], Xiang Xia(向 霞)[a)], Yuan Xiao-Dong(袁晓东)[b)], He Shao-Bo(贺少勃)[b)], Jiang Xiao-Dong(蒋晓东)[b)], Zheng Wan-Guo(郑万国)[b)], and Zu Xiao-Tao(祖小涛)[a)]

[a)] *Institute of Physics and Electronics, University of Electronic Science and Technology of China, Chengdu* 610054, *China*
[b)] *Research Center of Laser Fusion, China Academy of Engineering Physics, Mianyang* 621900, *China*

(Received 18 August 2012; revised manuscript received 17 October 2012)

The effect of defect density on the modulation of incident laser waves is investigated. First, based on the actual defect distribution in the subsurface of fused silica, a three-dimensional (3D) grid model of defect sites is constructed. The 3D finite-difference time-domain method is developed to solve the Maxwell equations. Then the electrical field intensity in the vicinity of the defect sites in the subsurface of fused silica is numerically calculated. The relationships between the maximal electrical field intensity in fused silica and the geometry of the defect sites are given. The simulated results reveal that the modulation becomes more remarkable with an increase of the defect density. In addition, the effect of the distribution mode of defects on modulation is discussed. Meanwhile, the underlying physical mechanism is analyzed in detail.

Keywords: defect site density, laser-induced damage, fused silica

PACS: 42.60.JF, 42.62.–b, 42.70.Ce, 46.15.–x **DOI:** 10.1088/1674-1056/22/5/054207

1. Introduction

Laser damage is one of the main limitations in the operation of high-power laser facilities.[1–4] As a laser irradiates optics, such as fused silica, a large number of damage sites are created as shown in Fig. 1.[5] Laser-induced damage in optics is a localized phenomenon associated with the presence of micron and sub-micron scale defects.[6,7] These defects can be absorbers or non-absorbers. In the latter case the damage may cause field enhancement and/or a reduction in heat conduction. Each, ultimately, can lead to material damage.[8] The damage threshold of optics used in inertial confinement fusion (ICF) lasers, where laser fluence can average more than 8 J/cm^2, is a key parameter used to predict the expected lifetime of ICF optics.[5,9] The existence of damage sites reduces the damage threshold of optics to a certain extent. Because the optics used in ICF are very expensive and there is a requirement for long service life,[10] it is necessary to investigate the damage mechanism theoretically and provide a theoretical direction to corresponding experiments.

As for the field enhancement caused by defects, there have been some reports. Génin *et al.*[11] numerically simulated the intensity distribution using TEMPEST code around the planar and conical cracks. Bonneau *et al.*[12] performed a two-dimensional (2D) simulation of intensity distribution around the planar and conical cracks by using DELPOR code and HESIONE code. Hua *et al.*[13] simulated the light intensity distribution in the vicinity of three dimensional Hertzian conical pits on fused silica subsurface. Li *et al.*[14–16] discussed the modulation of incident waves from a laser by Gaussian defects. Nevertheless, these simulations mainly focus on the electrical field enhancement around one defect or damage site. Few pay attention to the modulation arising from multiple defects and the effect of defect density on the modulation.

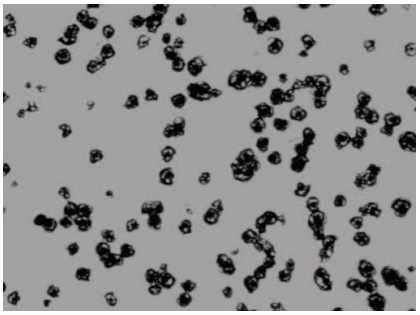


Fig. 1. Optical micrograph showing the spatial distribution of damage sites.[5]

In the present work, the density and different distributions of defect sites are considered. Three-dimensional (3D) grid models of defect sites are constructed first. Maxwell equations are solved by the 3D finite-difference time-domain method. Then the electrical field intensity distribution in the vicinity of the defect sites in the front subsurface of fused silica is numerically simulated. The relationships between the maximal electrical field intensity in fused silica and the geometry of the defect sites are discussed. This work aims to provide theoretical direction about the laser induced damage during ICF.

*Project supported by the Fundamental Research Funds for the Central Universities, China (Grant No. ZYGX2010J045), the National Natural Science Fundation of China and the China Academy of Engineering Physics United Foundation (NSFA) (Grant No. 11076008).

†Corresponding author. E-mail: jasmine2008@uestc.edu.cn

© 2013 Chinese Physical Society and IOP Publishing Ltd

2. Model and method

For simplicity, we assume each defect site is hemispherical, and has the radius r.[5] The 3D grid model of the defect site is built first. In the model, the surface of the defect site can be described by the 3D equation

$$(x-x_0)^2+(y-y_0)^2+(z-z_0)^2=r^2,$$

where the xoy plane is parallel to the fused silica surface, (x_0, y_0, z_0) is the center of the bottom of the defect. Figure 2 shows a 2D schematic of the 3D grid model of the hemispherical defect. The difference in grid size is $\delta=\lambda/12=29.25$ nm.

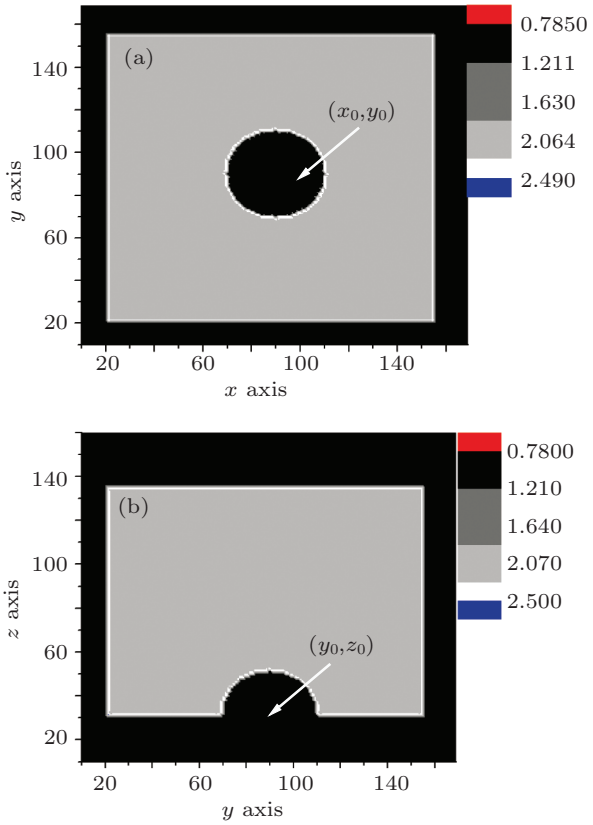


Fig. 2. (color online) The 2D schematic plots of the defect. (a) Plane $z=31$ h, (b) Plane $x=90$ h.

Maxwell's equations are solved by the 3D finite-difference time-domain method to calculate the electric field intensity distribution in the vicinity of the defect site.[17,18] During the numerical calculation, the perfectly matched layer (PML) boundary condition is adopted.[17] The relative dielectric constant ε_r of fused silica is 2.25. The 351 nm laser with an amplitude 1.0 V/m travels in the direction normal to the surface, namely along the z axis. The transverse magnetic (TM) wave is considered in this work. Other defects in the fused silica are ignored. It is assumed that the defect sites are on the front surface and the defects are empty ($\varepsilon_r=1.0$). In simulation, the size of the defect site is only about 10% of an actual one due to the limitation of present computer internal storage.

3. Results and discussion

In order to investigate the effect of defect site density on the modulation of the incident electrical field, we calculated the electrical field intensity of different planes in three cases: (i) one defect, (ii) two defects, and (iii) three defects existing in the incident subsurface of fused silica. The calculated results are shown in Figs. 3–10. The whole calculation domains of Figs. 3–10 is (215δ, 215δ, 115δ). In addition, the effect of the distribution modes of defects is studied as shown by Fig. 11 and Table 1. The whole calculation domain of Fig. 11 is (180δ, 180δ, 126δ).

3.1. One defect

Figures 3 and 4 refer to the case in which only one defect exists in a given domain. Figure 3 displays the electric field intensity distribution around a defect ($r=20\delta$) at plane $x=115\delta$. Since the laser is TM wave, the electric intensity along the x axis is shown. In Fig. 3, the electrical field is significantly scattered by the defect and the electrical field distribution is symmetrical. The phenomenon can be explained as follows. Since the defect is empty, it resembles a concave mirror located at the position of the defect site. The incident laser is scattered by the concave mirror behind the defect. Where scattering waves overlap incident waves, the electric field is intensified as a consequence of interference in the overlap.[19] When the laser irradiates the interface of the fused silica and the defect, some of the incident waves are reflected and overlap incident waves. So we find that the intensification appears not only behind the defect but also inside the defect. According to the calculation, the maximum electrical field intensity (E_{max}) at $x=115\delta$ is 1.99 V/m. The result of electrical field intensity is in good agreement with the calculated data of Refs. [11] and [15] in order of magnitude.

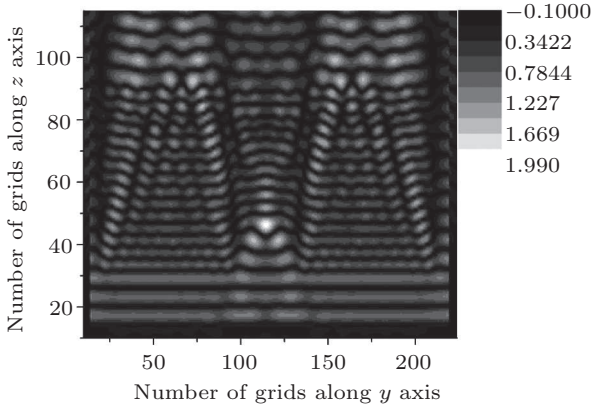


Fig. 3. Distribution of electrical field at $x=115\delta$.

Figure 4 is the evolution of E_{max} in fused silica with the radius of the hemispherical defect r. From Fig. 4, it can be observed that E_{max} increases with r quite irregularly in leaps

and bounds. As we all know, the larger r is, the wider the scattering domain is. And more waves interfere reciprocally. Accordingly, E_{max} is higher for larger r. Also we can see that the curve representing E_{max} in the rear surface $z = 100\delta$ is the highest. This rear surface effect is in good accord with the experimental results.[15,20]

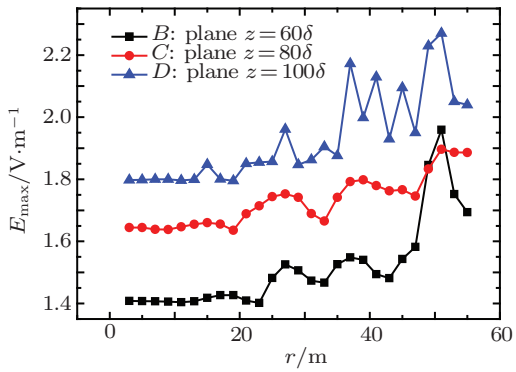


Fig. 4. (color online) Dependencies of E_{max} on defect radius r.

3.2. Two defects

In this section, we discuss the modulation of the electrical field by two hemispherical defects. Figure 5 is a 2D schematic plot of the two defects. The radii of the two defects are both 20δ. Figure 6 is the electrical field distribution at plane x=115δ. Comparing with Fig. 3, we can see an intensification domain around the line $y = 115\delta$ in Fig. 6. This is due to the overlap of the scattering waves of the two defects. E_{max} in Fig. 6 is 2.06 V/m.

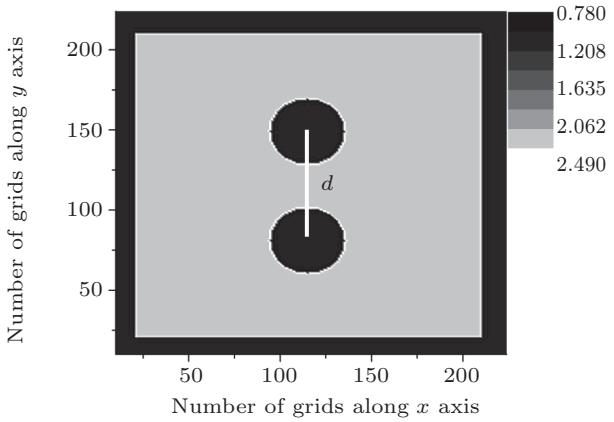


Fig. 5. 2D schematic plot of the defect.

Figure 7 demonstrates the evolution of E_{max} with the distance of two defects d in three xoy planes. It can be found that with the increase of d, E_{max} decreases slowly. The reason is obvious. As the two defects are close enough, interference may occur more than once due to the refection by the defects. However with the increase of d of two defects, the encounter probability of the scattering waves of each defect decreases. Certainly, the intensification attenuates with d.

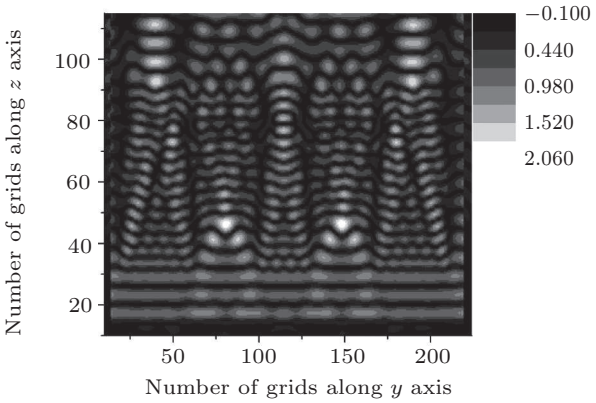


Fig. 6. Distribution of electrical field at $x = 115\delta$.

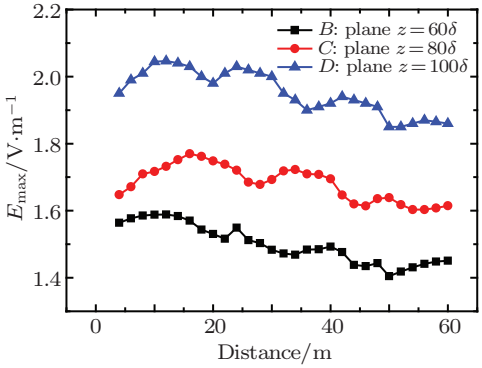


Fig. 7. (color online) Dependencies of E_{max} on the distance between two defects.

3.3. Three defects

In the actual optics subsurface, there are a number of defects in a given domain. So it is necessary to discuss the modulation of the electrical field by more than two defects. A grid model of three defects is shown in Fig. 8. The radii of the three defects are the same. The centers of the three defects define a circle with radius R.

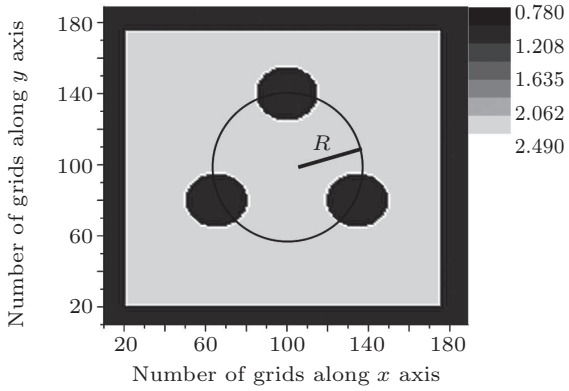


Fig. 8. 2D schematic plot of three defects.

Figure 9 refers to the electrical field distribution at plane $x = 115\delta$. The radii of the three defects are all 20δ. A remarkable characteristic of Fig. 9 is that the distribution of electric

field is disordered in a way compared with Figs. 3 and 6. The electric field distribution in Fig. 9 originates from the defect distribution at the plane $x = 115\delta$. The maximum electrical field intensity in Fig. 9 is 2.10 V/m.

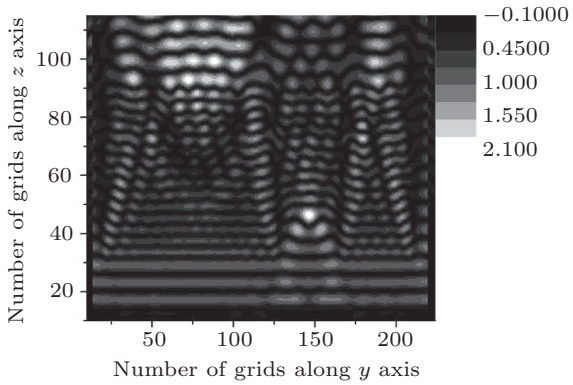


Fig. 9. Distribution of electrical field at $x = 115\delta$.

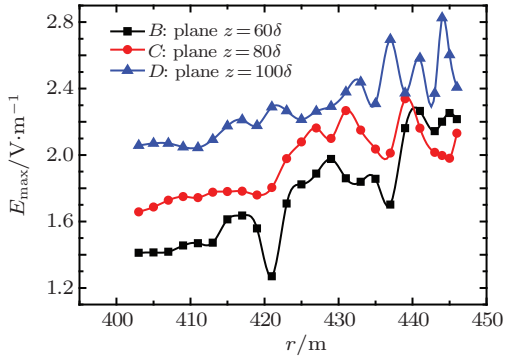


Fig. 10. (color online) Dependencies of $E_{\max}$ on defect diameter r.

In addition, the effect of defects geometry on electrical field modulation is investigated. Figure 10 shows the evolution of $E_{\max}$ with the radius r of the three defects. It can be observed that $E_{\max}$ increases with r irregularly with some leaps. According to our calculation, the average of $E_{\max}$ of curve D ($z = 100\delta$) in Fig. 10 is about 2.4 V/m, which is somewhat higher than the average of curve D ($z = 100\delta$) in Fig. 4 (about 2.0 V/m). This phenomenon reveals that the modulation of three defects is greater than that of one defect.

So far, we have investigated the modulation by different numbers of defects (or by different defect densities). A significant conclusion is that the modulation becomes more remarkable with the increases of the defect density and the sizes of defects.

3.4. The effect of distribution mode on modulation

In order to consider our model from other perspectives, we discuss the effect of two defect distribution modes on modulation. Figures 11(a), 11(c), and 11(e) show the electric field distribution centered on three craters in a line, figures 11(b), 11(d), and 11(f) show the electric field distribution centered on three craters in a circle. The radius of each defect is 20δ. For the two distribution modes, the defect densities can be regarded as the same in a given area $S = \pi(R+r)^2 m^2$.

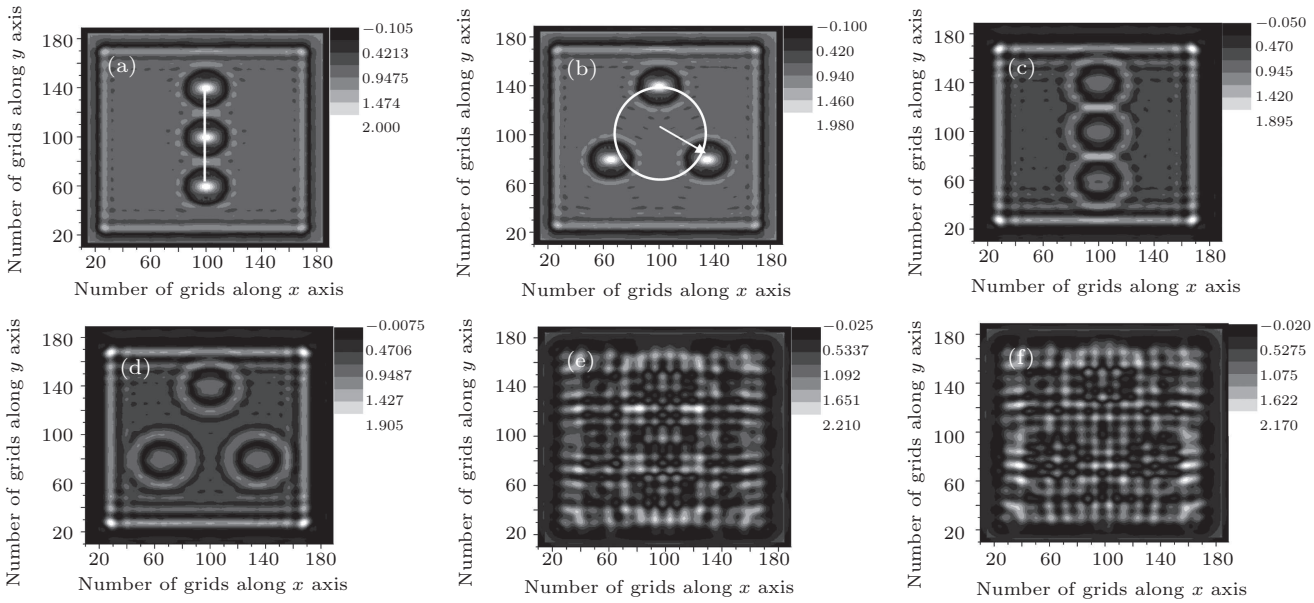


Fig. 11. Electrical field distribution centered on (a) three craters in a line with $z = 50\delta$, (b) three craters in a circle with $z = 50\delta$, (c) three craters in a line with $z = 80\delta$, (d) three craters in a circle with $z = 80\delta$, (e) three craters in a line with $z = 100\delta$, and (f) three craters in a circle with $z = 100\delta$.

Figures 11(a) and 11(b) refer to the electric field distribution in plane $z = 50\delta$. It can be seen that the greatest enhancement appears in the center of each defect in both Figs. 11(a) and 11(b). Figures 11(c) and 11(d) refer to the electric field distribution in plane $z = 80\delta$. We can observe that the $E_{\max}$ appears at the fused silica boundary. The difference between

Figs. 11(c) and 11(d) is that there are intensification domains between defects in Fig. 11(c) while there are no such intensification domains in Figs. 11(d), 11(e), and 11(f) refer to the electric field distribution in plane z=100δ, which is the rear surface of the fused silica. In both Figs. 11(e) and 11(f), there is an enhanced domain around the shadow of each defect in the rear surface.

Table 1 shows the $E_{\max}$ of Fig. 11(a) to Fig. 11(f). We can see an interesting phenomenon. In spite of the variation of the electric field distribution of Fig. 11(a) to Fig. 11(f), the $E_{\max}$ for the two defect distribution modes in a given plane do not differ much. That is to say, the modulation is not very sensitive to the defect distribution mode when the defect density is same.

Table 1. The $E_{\max}$/V·m^{-1} for the two modes of three defects according to Fig. 11.

	$z=50\delta$	$z=80\delta$	$z=100\delta$
Distribution in a line	Fig. 11(a): 2.00	Fig. 11(c): 1.895	Fig. 11(e): 2.21
Distribution in a circle	Fig. 11(b): 1.980	Fig. 11(d): 1.905	Fig. 11(f): 2.17

4. Conclusions

With the above discussion, several conclusions are obtained.

(i) With the radius of hemispherical defect increasing, the modulation increases. With the increase of defect separation distance, the modulation becomes gentler. The rear surface effect is very remarkable.

(ii) The larger the defect density is, the stronger the modulation is.

(iii) If the defect density is constant, the modulation is not very sensitive to the defect distribution mode.

References

[1] Deng H X, Zu X T, Xiang X and Sun K 2010 *Phys. Rev. Lett.* **105** 113603

[2] Carr C W, Radousky H B, Rubenchik A M, Feit M D and Demos S G 2004 *Phys. Rev. B* **92** 087401

[3] Lamaignere L, Donval T and Loseau M 2009 *Meas. Sci. Technol.* **20** 095701

[4] Bercegol H, Bouchut P R and Lamaignere L 2004 *Proc. SPIE* **5273** 312

[5] Matthews M J and Feit M D 2007 *SPIN* UCRL-PROC-236247

[6] Walker T W, Guenther A H and Nielsen P 1981 *IEEE J. Quant. Electron.* **QE-17** 2053

[7] Papernov S and Schmid A W 1997 *J. Appl. Phys.* **82** 5422

[8] Wu Z L, Feit M D, Kozlowski M R, Rubenchik A M and Sheehan L 1998 *Proc. SPIE* **3578** 721

[9] Moses E I 2005 *IEEE Int. Conf. on Plasma Sci. ICOPS* 2005 (California: IEEE) TUAI001

[10] Matthews M J, Bass I L, Guss G M, Widmayer and Ravizza F L 2007 *Proc. SPIE* **6720** 67200A

[11] Génin F Y, Salleo A, Pistor T V and Chase L L 2001 *Opt. Soc. Am. A* **18** 2607

[12] Bonneau F, Combis P, Pujols A, Rullier J L, Seques M and Vierne J 2003 *Proc. SPIE* **4932** 250

[13] Hua J R, Zu X T, Li L, Xiang X, Chen M, Jiang X D, Yuan X D and Zheng W G 2010 *Acta Phys. Sin.* **59** 2519 (in Chinese)

[14] Li L, Xiang X, Zu X T, Jiang X D, Yuan X D and Zheng W G 2011 *Optik* **122** 1423

[15] Li L, Xiang X, Zu X T, Wang H J, Yuan X D, Jiang X D, Zheng W G and Dai W 2011 *Chin. Phys. B* **20** 074209

[16] Li L, Xiang X, Zu X T, Yuan X D, He S B, Jiang X D and Zheng W G 2012 *Chin. Phys. B* **21** 044212

[17] Ge D B, Yan Y B 2002 *Electro-magnetic Wave and Finite-Difference Fince-Dorucion* (Xi'an: Xidian University Press)

[18] Sullivan D M 2000 *Electromagnetic Simulation Using the FDTD Method* (New York: IEEE Press)

[19] Welford W T 1981 *Optics* (New York: Oxford University Press)

[20] Crisp M D, Boling N L and Dube G 1972 *Appl. Phys. Lett.* **21** 364